Journal of King Saud University – Science 35 (2023) 102753

HOSTED BY

Contents lists available at ScienceDirect

Journal of King Saud University – Science

journal homepage: www.sciencedirect.com

Original article

An evaluation of the biological activity of zinc oxide nanoparticles fabricated from aqueous bark extracts of *Acacia nilotica*

Manoharan Janani [a], Thandapani Gomathi [b], Ranganathan Babujanarthanam [c,*], K. Kaviyarasu [d,e,*]

[a] Department of Biochemistry, Auxilium College (Autonomous), Gandhi Nagar, Vellore 632006, Tamil Nadu, India
[b] Department of Chemistry, D.K.M College for Women (Autonomous), Vellore 632006, Tamil Nadu, India
[c] Nano and Energy Bioscience Laboratory, Department of Biotechnology, Thiruvalluvar University, Serkkadu, Vellore 632115, Tamil Nadu, India
[d] UNESCO-UNISA Africa, Nanosciences/Nanotechnology Laboratories, College of Graduate Studies, University of South Africa (UNISA), Muckleneuk Ridge, PO Box 392, Pretoria, South Africa
[e] Nanosciences African Network (NANOAFNET), Materials Research Group (MRG), iThemba LABS-National Research Foundation (NRF), 1 Old Faure Road, 7129, PO Box 722, Somerset West, Western Cape Province, South Africa

ARTICLE INFO

Article history:
Received 22 June 2022
Revised 29 May 2023
Accepted 5 June 2023
Available online 13 June 2023

Keywords:
Acacia nilotica
Fungicidal
Antiradical
Cytotoxic
Larvicidal
Biofilm

ABSTRACT

The phyto nanotechnology strategy was executed for the genesis of zinc oxide nanoparticles by applying bark aqueous extract of *Acacia nilotica* (AN-ZnO NPs). The AN-ZnO NPs emergence was substantiated through a distinct peak at 350 nm in the ultraviolet–visible spectroscopy. The fourier transform infrared spectroscopy exposed the phyto-organic moieties engaged as reduction and stabilization factors in fabricating nanoparticles. The crystalline trait, elemental proportions, spherical and hexagonal geometry of AN-ZnO NPs was witnessed by X-ray diffraction, energy-dispersive X-ray analysis and scanning electron microscopy. The high-resolution transmission electron microscopic technique provided the average size of 35 nm. AN-ZnO NPs presented larger inhibition zone against *Candida albicans* (22.7 ± 0.32 mm) at 40 μg/mL as an effectual fungicidal agent. Execution of in vitro antiradical scavenging assay of AN-ZnO NPs applying 2,2-diphenyl-1-picrylhydrazyl (DPPH), nitric oxide (NO), hydroxyl radical (OH^-), 2,2′-azin o-bis-(3-ethylbenzothiazoline-6-sulphonic acid) displayed radical scavenging trait with the minimum inhibitory concentration (IC_{50}) of 34.54 μg/mL, 38.0 μg/mL, 41.34 μg/mL, and 35.41 μg/mL, respectively. Cytotoxic feature against MCF-7 cell line was in a dose-manner with IC_{50} value of 37.15 μg/mL in addition to apoptotic proteins expressions were displayed by AN-ZnO NPs. An appreciable larvicidal role of AN-ZnO NPs was rendered against *Anopheles stephensi* with LD_{50} (0.31 ppm) and LD_{90} (0.59 ppm), besides acetylcholinesterase inhibition. Further, biofilm origination was remarkably ceased by the *Staphylococcus aureus* and *Klebsiella pneumoniae*, respectively. All our experimented reports on AN-ZnO NPs attested the credible applicability of ZnO NPs in biomedical care for health troubles.

1. Introduction

Nanotechnology is stupendously developing with the urge to fabricate desired nanometric particles (1–100 nm) by shaping multifarious bulk materials offering elite physio-chemical traits like exceptional greater surface-area, chemical stableness, catalytic and optoelectronic features. Thus, booming in its appreciative role in nano-biomedicine (Patil and Chandrasekaran, 2020; Mayedwa et al., 2018). Distinct physical and chemical (synthetic) methodologies were practiced to speedily tailor the nanoparticles. The need for higher energy, non-biodegradability, and adherence of noxious solvents over the nanoparticles makes them unsuitable for the bio-nanomedicine due to aftermath impression on human health. These aforesaid hurdles have engrossed for the alternative eco-sustainable methodologies to fabricate nano-sized particles (Khandel et al., 2018). Bio-inspired fabrication of nanoparticles is in the current spotlight, using natural living entities like microbes (bacteria, algae, and fungi) and varying sections of plants (stem, bark, flower, seed, etc.). Sterile culture media for microbes were obviated by the adopting plants in the genesis of nanoparticles (Punniyakotti et al., 2020; Ezhilarasi et al., 2019). The profusely stuffed bio-organic entities in the plants like polyphenolics and other active moieties are indulged in reducing and stabilizing nanoparticles by adhering to the metal ions. Size amenability, huge scale fabrication, steadiness, low-budget, safety, and eco-sustainability are merits of phyto-inspired fabrication

* Corresponding authors.
E-mail addresses: babukmg@gmail.com (R. Babujanarthanam), kavi@tlabs.ac.za (K. Kaviyarasu).

https://doi.org/10.1016/j.jksus.2023.102753
1018-3647/

(Jegadeesan et al., 2019). Already, inorganic metallic forms of nanoparticles such as titanium, silver, gold, zinc, nickel, palladium, and copper have been massively produced and adopted in biomedical applications from plant origin (Kuppusamy et al., 2016; Valsalam et al., 2019).

Amid extensive groups of metal or metallic oxide nanoparticles, zinc oxide (ZnO) nanoparticles (NPs) with distinguished and impressive piezoelectric, optical, and magnetic features have made its pertinence as a multifaceted metal oxide nanoparticle. Furthermore, the biological safety, chemical steadiness, and biocompatibility aspects of ZnO NPs have put forward their enormous applicability in medicinal nanoscience to mitigate myriad health maladies. The proposed therapeutics include antimicrobial, antidiabetic (Rajeswari et al., 2018); tissue engineering (Khader and Arinzeh, 2020); wound healing (Gao et al., 2017) and drug nanocarrier (Sundraraman and Jayakumari, 2020). The inevitable aerobic mechanism within the cells engenders free radicals as a natural by-product. A milder concentration of free radicals is crucial for immune responses. Reactive free radicals have havocking effect when overwhelmed within the biological system by supporting oxidative stress and fostering deformation of vital bio-organic structures that include lipid, nucleic acid, and proteins. Consequently, implicating numerous health complaints, such as heart problems, cancer, neurodegenerative disorders, and diabetes mellitus. Antioxidants from the natural platform are supreme to synthetic antioxidants (Mani et al., 2021). Medicinal plants with secondary phyto-metabolic active chemicals are stupendous natural antioxidants (Mani et al., 2021; Mani et al., 2021).

In the human race, fungal infections outline the chief burden. Antimycotic agents practiced topically for dermal or other infections can provoke the frequency of toxicity, a lesser biological availability, itching and allergic skin responses. Metallic nanoparticles holding diminutive dimensions and modified features are in the task as a novel system of drug carriers with efficient desirability (Senguttuvan et al., 2014). Globe wide, cancer is the prime concerned for health complications and evidenced for major mortality in both higher and lower-income countries, despite the sophisticated diagnostic and therapeutic tools availabilities (Garg et al., 2020). In females, breast cancer is the paramount reason of death. The utility of the chemotherapeutic regimen had substantiated the problem of toxicity to the unrelated tissues, especially gastrointestinal and neurotoxicity (Angel Ezhilarasi et al., 2018). Nanoparticles tailored through a greener protocol have become the newer viewpoint as nanotherapeutics for neoplastic diseases (Subramanian et al., 2013).

Mosquitoes (Sathiyaraj et al., 2022) are the extremely deadly arthropod vectors that are indulged in transmitting diseases to humans such as yellow fever, filariasis, malaria, dengue, and Japanese encephalitis. As scrutinized by the WHO (World Health Organization (WHO), 2005. WHO/CDS/2005.26.), malaria is involved in greater mortality in all age groups. The tremendous resistance to insecticides on mosquitoes, toxicity to the nonrelated organism in the ecosystem and human illness issues has necessitated the affordable, novel, and unfailing strategies for mosquito lysis. The pristine and miscellaneous compounds acquired from plants function as furious bio-reducers and stabilizer agents in the emergence of metallic nanoparticles with an intense larvicidal trait. Plant-inspired metallic nano-larvicides are the nonhazardous and cheapest protocols to eradicate mosquitoes. Biofilms developed by the bacterial communities are a menace to humans as they colonize dramatically over the exterior of medical instruments, rooting lung infections (tuberculosis), dental caries, chronic osteomyelitis, urinary tract infections and chronic wounds. The resistibility of microbial strains to commercially usable synthetic antibiotics is the foremost threat now. There is an urgency for the innovation of newer drugs with utmost efficacy to combat the complications. Phyto-chemicals in curative plants and nano-based metallic particles are alternative origin to exterminate infectious population. *Acacia nilotica* (*A.nilotica*) in the Fabaceae family is an imperatively medicinally valued tree. It is also designated as Babul, Indian gum Arabic or Kikar and dispersed vastly in India, Africa, and Middle Eastern countries. The ayurvedic system adopts varying sections of the tree to eradicate human maladies such as earache, microbial infections, bleeding piles, cancer, and diabetes. Surplus tannin in the bark has an astringent trait. The bark decoctions are applied to cure mouth cancer, uterus prolapse, leucorrhoea and syphilis diseases. Antioxidant, anti-hypertensive, antiplasmodial and anti-inflammatory traits are also delineated in *A. nilotica*.

2. Experimental section

2.1. Collection, authentication, and processing of bark

The bark of the medicinally valued *A.nilotica* (specimen) was collected from Gudiyattam, Vellore district, Tamil Nadu, India. The bark was scrapped with a sterile knife from the trunk section of a healthful disease-free tree. The taxonomy and identity of the selected tree (Voucher No: PARC/2021/4512) was validated at the Herbal Plant Anatomy Research Centre (PARC), West Tambaram, Chennai and the voucher was preserved. The bark section collected was surface cleaned recurrently with surplus distilled water to eradicate grimy materials, shade dried to achieve a steady mass and incised into tiny pieces. Subsequently, powdered in a home blender, sieved, and placed in an airtight jar at ambient temperature for all experimental investigations.

2.2. Bark extract preparation

The bark extract for the reduction and stabilizing of nanoparticle's synthesis was prepared under sterile condition. Exactly, 3 g of powdered bark material was placed into a 250 mL Erlenmeyer flask containing 100 mL of double distilled water and extraction was accomplished with persistent stirring on a hot plate magnetic stirrer at 60 °C for 20 min. The solution was cooled, and double filtration was done using Whatman No.1 filter paper. The obtained clear, yellow-brownish coloured aqueous bark extract was taken to synthesize zinc oxide nanoparticles (ZnO NPs).

2.3. Qualitative screening of bark of A.nilotica

Applying the already availed standard protocol, scrutinization of existing phytochemicals was done (Rawani, 2017).

2.4. Phyto-based fabrication of zinc oxide nanoparticles

For harnessing ZnO NPs, exactly, 20 mL of bark extract of *A.nilotica* was vigorously stirred with 80 mL of 20 mM zinc nitrate hexahydrate [Zn $(NO_3).6H_2O$] on a magnetic stirrer (600 rpm) at 60 °C for 4 hrs and kept undisturbed, followed by 24 hrs incubation. The settled muddy-coloured precipitate was centrifuged for 20 min at 10000 rpm. The pellet was triple washed with ethanol and double distilled water to eliminate impurities bound to the nanoparticles. The purified zinc oxide nanoparticles pellet was dried in an oven within 70–80 ℃, made into a fine powder and calcinated in a muffle furnace at 400 ℃ for 2 hrs. The acquired zinc oxide nanoparticles from *A.nilotica* bark extract were designated as AN-ZnO NPs and retained in a sterile vial. The physiochemical characterization of nanoparticles was executed with advanced analytical and microscopic tools.

2.5. Physicochemical characterization of AN-ZnO NPs

2.5.1. UV–visible spectroscopy of AN-ZnO NPs

The colour conversion on blending thoroughly the bark extract of *A.nilotica* with zinc nitrate was assessed visually. Through periodic sampling of aliquots (2–3 mL), the biogenic reduction of zinc ions into AN-ZnO NPs in the aqueous reaction solution was checked. The maximum spectral absorption was executed from 200 to 800 nm in a UV–Visible spectrophotometer (JASCO V-670 PC UV–Visible spectrophotometer).

2.5.2. Fourier transform infrared (FTIR) spectral analysis of AN-ZnO NPs

The phytometabolites, their functional groups and chemical bonds existing in *A.nilotica* to reduce and stabilize the AN-ZnO NPs were verified in the unique spectra formed in the FTIR. Potassium bromide was mingled with AN-ZnO NPs to acquire the pellet under a hydraulic pellet machine, then placed within the sample holder and the scanning wavelength was ranged from 400 cm^{-1} to 4000 cm^{-1} at 4 cm^{-1} (resolution) in the Nicolet iS50 (Thermo Fischer Scientific) FTIR.

2.5.3. Powdered X-ray diffraction (P-XRD) spectral assessment of AN-ZnO NPs

The crystallographic fingerprint and purity phase of AN-ZnO NPs were keenly assessed through powdered XRD. The X-ray diffraction was enforced adopting a Bruker D8 Advance X-ray diffractometer with CuK_{α} radiation, 2 theta range ($20^{\circ} - 80^{\circ}$) handled at 30 kV with 10 mA (0.5 s). The crystallite dimension of the fabricated AN-ZnO NPs was pointed out using Debye-Scherrer's formula as mentioned, $D = 0.89\lambda/\beta\cos\theta$. Here, the crystallographic size (nm) of nanoparticles was denoted to be D, wavelength of the used X-ray as λ (lambda = 1.5406 Å), FWHM (full width at half maximum) as β and Bragg's angle of diffraction as θ.

2.5.4. SEM and EDX analysis of AN-ZnO NPs

The surface morphological features of engineered AN-ZnO NPs was assessed in JOEL 6390LA scanning electron microscope (SEM). On a copper grid coated with carbon, a thin layer of AN-ZnO NPs was placed, dried under a mercury lamp and the imaging was done with magnification. The purity of AN-ZnO NPs, qualitatively existed elements were resolved in Energy Dispersive X-ray analysis (EDX) integrated with the scanning electron microscope.

2.5.5. High-resolution transmission electron microscopy (HRTEM) and selected area electron diffraction (SAED) of AN-ZnO NPs

The nanostructure, geometry, and dimension of the AN-ZnO NPs were reported by the FEI-Tecnai G2 20 Twin high-resolution transmission electron (HRTEM) microscopic technique operated at a voltage of 80 kV. The ethanol sonicated suspension (4 µL) of AN-ZnO NPs was coated over the copper-carbon coated grid and scrutinized for surface morphology under the microscope. *Image J Software* (1.45 s) was used to evaluate the size of the nanocrystals. To further confirm the crystallinity of nanoparticles, the SAED (selected area electron diffraction) pattern was also recorded with HRTEM.

2.6. Antifungal susceptibility of AN-ZnO NPs

A classic well diffusion protocol was applied to check the fungicidal property of AN-ZnO NPs on randomly chosen six pathogenic fungal strains namely, *Aspergillus niger* (MTCC-9652), *Aspergillus flavus* (MTCC-873), *Rhizopus oryzae* (MTCC-9605), *Candida albicans* (MTCC-4748), *Microsporum gypseum* (MTCC-2830) and *Trichophyton rubrum* (MTCC-7859). Appropriately, 100 µL of each fungal strain inoculum was carefully swabbed over the solidified surface of the potato dextrose agar medium taken in a sterile individual petri-plates with a L-shaped glass rod. With the aid of a sterile gel borer (6 mm) wells were made within the PDA medium and AN-ZnO NPs with varying concentrations (10 µg/mL, 20 µg/mL, 30 µg/mL and 40 µg/mL) were placed into the wells using a micropipette and incubated for 2–4 days at room temperature. The fungicidal potentiality of the AN-ZnO NPs was visualized by measuring the inhibition zone width (in terms of mm). Amphotericin B at 10 µg/mL was utilized as a drug of positive control.

2.7. Antiradical assay of AN-ZnO NPs

2.7.1. 2, 2-diphenyl-1-picrylhydrazyl (DPPH) scavenging assay

The antiradical potential of phyo-inspired harnessed AN-ZnO NPs was assessed using the DPPH (2,2-diphenyl-1-picrylhydrazyl) method as previously documented with minor variations. At first, 1 mL of synthesized AN-ZnO NPs in a diverse range of concentrations (20 µg/mL to 60 µg/mL) were individually combined with the DPPH of 4 mL prepared as 0.004% solution in methanol and kept undisturbed at the ambient temperature in a dark condition for 30 min. The absorbance of the faded purple colour of DPPH to yellow colour was recorded spectrophotometrically at 517 nm. The AN-ZnO NPs reports were compared to the standard reference solution of ascorbic acid. As a blank, methanol was used. The radical quenching ability was calculated in percentage (%) as mentioned in the below-provided equation.

$$\text{DPPH radical quenching ability}(\%) = \left[\left(C_{(Abs)} - S_{(Abs)}\right)/C_{(Abs)}\right] \times 100$$

Here, $C_{(Abs)}$ - Control (DPPH in methanol) absorbance, $S_{(Abs)}$ - AN-ZnO NPs/Ascorbic acid (along with DPPH) absorbance. The sample concentration offering 50% antiradical ability (IC_{50}) was also calculated.

2.7.2. Nitric oxide (NO) scavenging assay

The Griess reaction was adopted to quantify the nitrite ions produced due to the interaction of an aqueous solution of sodium nitroprusside with oxygen, as earlier prescribed by Sylvie *et al.*, (Sylvie et al., 2014) including a few alterations. Nitric oxide (NO) scavenging activity was screened for AN-ZnO NPs. About 20 µg/mL to 60 µg/mL concentrations of AN-ZnO NPs (each 1 mL) were well blended in separate test tubes with 2 mL of 10 mmol/L of sodium nitroprusside solution prepared using 50 mmol/L of phosphate buffer (pH 7.4). The reaction tubes were incubated for nearly 150 min at ambient temperature. Subsequently, added one mL of 0.33% of sulfanilic acid (diluted in 20% glacial acetic acid) to the reaction mixture (0.5 mL) and left for diazotization for 5 min. Before incubation for 30 min, 1 mL of 0.1 % napthylethylenediamine dihydrochloride was reacted to the test tube contents. Spectrophotometrically, the developed chromophore (pink colour) intensity was recorded at 540 nm. Ascorbic acid served as a positive reference. The blank solution was methanol. The below-provided formula was implemented to calculate the % (percentage) of reduction in nitric oxide radical by AN-ZnO NPs.

$$\%\text{Radical(NO)reduction} = \left[\left(C_{(Abs)} - S_{(Abs)}/C_{(Abs)}\right)\right] \times 100$$

Here, $C_{(Abs)}$ - Control (without AN-ZnO NPs) absorbance, $S_{(Abs)}$ - AN-ZnO NPs /Ascorbic acid absorbance. IC_{50} value was also computed.

2.7.3. Hydroxyl radical scavenging (OH^{-}) assay

The scavenging potentiality of AN-ZnO NPs on the hydroxyl radical (OH^{-}) was executed with the protocol implemented by Subramanian *et al.*, (Gupta et al., 2015). Initially, 0.2 mL of AN-ZnO NPs of varied ranges (20 µg/mL to 60 µg/mL) were added into the inde-

pendent test tubes along with 1 mL solution of EDTA (0.13 % of anhydrous ferrous ammonium sulphate with 0.26 % of EDTA diluted in 100 mL of distilled water) and completely blended with 0.85 % of DMSO (1 mL) in phosphate buffer of 0.1 M (pH 7.4) to trigger the reaction. Subsequently, 0.22 % of ascorbic acid (0.5 mL) was further added into the reacting mixture. The contents were boiled within the water bath for 15 min at 90 ℃. Termination in the reaction was done by pouring 17.5 % of ice-cold trichloroacetic acid (1 mL), 3 mL of Nash reagent (75 % of ammonium acetate, 2 mL of acetylacetone and 3 mL of glacial acetic acid were combined, and volume was brought to 1 L using distilled water) was poured into all reaction tubes, incubated at room condition for 15 min. The yellowish chromophore obtained was spectrophotometrically recorded at 412 nm. Ascorbic acid was utilized as positive reference control and without ascorbic acid, the reaction mixture served as a negative control. By implementing the below-provided formula, the hydroxyl radical scavenging capacity of AN-ZnO NPs was calculated.

$$\text{Percentage of } OH^{-}\text{radical scavenged} = \left[\left(C_{(Abs)} - S_{(Abs)}/C_{(Abs)}\right)\right] \times 100$$

Here, $C_{(Abs)}$ – Control (without AN-ZnO NPs) absorbance, $S_{(Abs)}$ – AN-ZnO NPs/ Ascorbic acid absorbance. IC_{50} value was also computed.

2.7.4. ABTS (2,2′-Azino-bis (3-ethylbenzothiazoline-6-sulfonic acid) radical scavenging assay

The protocol of the ABTS scavenging assay of AN-ZnO NPs was executed with slight variations as done by Kuppurangan *et al.*, (Kuppurangan et al., 2016). By mingling an equal proportion of 7 mM solution of ABTS with 2.4 mM of potassium persulphate, a working solution was obtained and retained in a dark place for 12 h in room condition. Next, 1 mL of the resultant solution was thoroughly mingled with 1 mL of varying concentrations (20 μg/mL to 60 μg/mL) of AN-ZnO NPs. Six minutes later, the reacted mixture was read spectrophotometrically at 734 nm. The aptness of AN-ZnO NPs to scavenge ABTS was found out in percentage (%) by applying the below indicated formula:

$$\text{Percentage of ABTS inhibition} = \left[\left(C_{(Abs)} - S_{(Abs)}\right)/C_{(Abs)}\right] \times 100$$

Here, $C_{(Abs)}$ - Control (without AN-ZnO NPs) absorbance, $S_{(Abs)}$ - AN-ZnO NPs /Ascorbic acid absorbance. IC_{50} value was also computed.

2.8. Cytotoxic assay

2.8.1. Culture

The MCF-7 (Breast cancer cell line) was procured from NCCS (National Centre for Cell Science, Pune, India) and cultured in DMEM medium acquired from (Sigma-Aldrich, India), also boosted with 10% FBS (fetal bovine serum), 20 mL of antibiotic penicillin (1% w/v). The cells were sustained in an atmosphere of CO_2 (5%) with humidification (95%) at 37 ℃.

2.8.2. MTT -mediated cytotoxic evaluation of AN-ZnO NPs

MTT (3-(4,5-dimethylthiazol-2yl)-2,5-diphenyltetrazolium bromide) assay was executed for AN-ZnO NPs on MCF-7 (Breast cancer cell line) cell line as previously performed by Menon *et al.*, (Menon and Shanmugam, 2020). Exponentially proliferating MCF-7 cells (10^5 cells/well) were aseptically placed into the 96-well cell-culture plate and left undisturbed for 24 h in 5% CO_2 at 37 ℃ for 1 day to acquire confluency. Diverged concentrations of prepared AN-ZnO NPs (10 μg/mL to 90 μg/mL) were exposed to the MCF-7 cells, re-incubated for 24 h at 37 ℃ respectively. Next, 100 μL of 0.5% MTT (1 mg/mL) diluted in PBS was included to all the wells and re-incubated for 4 h at ambient condition. The supernatant MTT solution used was discarded. Using PBS, cells were washed. The finally procured purplish coloured crystals of formazan were diluted in dimethyl sulfoxide (100 μL). The value of absorbance was monitored at 570 nm with the aid of ELISA plate reader for each concentration. The inhibition of cell viability percentage (%) was computed using the below-mentioned formula:

$$\text{Cell viability}(\%) = [(A_{570}\text{value of tested cells}/A_{570}\text{value of control cells}) \times 100]$$

2.8.3. Determination of ROS using DCFH-DA (Dichlorodihydrofluorescein diacetate method)

The in vivo ROS emergence in the MCF-7 cells on treatment with AN-ZnO NPs was assessed the using DCFH-DA staining protocol. The non-fluorescent DCFH-DA dye on interaction with the ROS generates a fluorescent compound DCF (2′,7′-dichlorofluorescein). In brief, 1×10^5 MCF-7 cells/well were carefully laid into a microplate with 6-well. The MCF-7 cells were reacted with IC_{50} concentration of AN-ZnO NPs for 24 h and 48 h within the CO_2 incubator. DCFH-DA stain (10 μM) was exposed to the cultured cells and further incubated for 30 min at room temperature (37 ℃). Consequently, the reacted cells were double washed with cold phosphate buffer saline (PBS) and resuspended in PBS. Analysis of cells (reacted and unreacted) was performed beneath the fluorescence microscopic technique (40 X objective). Doxorubicin (500 μg/mL) was utilized as a positive control. The fluorescence intensity was read with a fluorescence microplate reader at excitation (485 nm) and emission (550 nm) respectively.

2.8.4. Analysis of mitochondrial membrane potential (MMP) using Rhodamine 123 staining

In brief, MCF-7 cells (1×10^5 cells/well) were placed into the 6-well microplate. AN-ZnO NPs at their respective IC_{50} concentration was reacted to the MCF-7 cells and left undisturbed. After 24 h and 48 h, the reacted cells were carefully harvested and using PBS rinsed twice. Then the cells were exposed to Rhodamine-123 dye (Rh-123; 10 μg/mL) for 30 min at 37 ℃ in a dark condition inside the CO_2 incubator and re-rinsed using PBS. At last, the intensity of fluorescence given by the Rh-123 stain was visualized with a fluorescent microscope and photographs of the treated cells as well as untreated cells (negative control) along with doxorubicin (500 μg/mL) positive control were captured. The pattern of depolarization in the mitochondrial membrane was seen. The fluorescence intensity was read with a fluorescence microplate reader at excitation (485 nm) and emission (550 nm), respectively.

2.8.5. Morphological assessment of nucleus using DAPI

The condensation of chromosomes in the apoptotic cells was identified by DAPI (4,6-diamidino-2-phenylindole), a fluorescent probe specific to the nuclei. The MCF-7 cells treated with AN-ZnO NPs (IC_{50} concentration) were incubated for 24 h and 48 h. Then, using PBS (phosphate buffer solution) the cells were repeatedly washed and fixed with formaldehyde (4%). Using DAPI solution (1 μg/mL) the cells were stained and left at 37 ℃ for 5 min. MCF-7 cells without AN-ZnO NPs exposure were utilized as a negative control whereas doxorubicin (500 μg/mL) exposed cells as a positive control. The cells were finally washed using PBS and the morphology of the nucleus was visualized under a fluorescence microscope with a blue filter (420 nm).

2.8.6. Western blotting technique

To detect the apoptotic (Bax, Caspase-3 and Caspase-9) and antiapoptotic expression of proteins (Bcl-2) along with proliferative protein marker expression (Cyclin D1 and PCNA) in the MCF-

7 cells (1 x10^5 density) exposed to AN-ZnO NPs were taken for western blot technique. MCF-7 cells cultured in 6-well tissue culture plates were reacted to AN-ZnO NPs (IC_{50} concentration) for 24 h and 48 h. In this blot assay, β-actin served as a standard loading control. At the end of incubation time, harvesting of cells was done utilizing RIPA lysis buffer solution and then quantified protein concentration spectrophotometrically. Electrophoresis of protein was executed from the collected sample in 12% SDS-PAGE (sodium dodecyl sulphate -polyacrylamide gel electrophoresis). Transfer of proteins from the gel onto nitrocellulose membrane was carried out and the membrane was blocked with 5% BSA (bovine serum albumin) for 1 h to hinder non-specific binding. The membrane was exposed to primary mAb (monoclonal antibodies) and left for 24 h at 4 ℃. A gentle washing of the membrane using TBST buffer was done, then secondary antibodies were reacted to the membrane and re-incubated for 1 h at ambient condition. At last, the membrane was thoroughly washed in TBST buffer and the levels of expression of proteins were detected with the aid of a chemiluminescent detection system (Biorad, USA).

2.9. Larvicidal efficacy of AN-ZnO NPs

The larvicidal efficacy of AN-ZnO NPs was accomplished with a standard methodology as applied by the WHO and Rawani *et al.,* (Rawani, 2017) with minor changes. For the larvicidal bioassay test, five sets of targeted 3rd instar larvae of *Anopheles stephensi* (100 larvae/set) were taken. For each concentration of test sample, one set was used. In a sterile 250 mL glass beaker, insertion of 100 mosquito larvae in 200 mL of AN-ZnO NPs solution of desired concentrations (0.1, 0.2, 0.3, 0.4 and 0.5 ppm)) were implemented. Each performed test was incorporated with a control group (distilled water). No feed was given to the larvae during the assay. Mortality was noted after 24 h post-treatment to the AN-ZnO NPs. The total number of dead larvae divided by the number of alive larvae multiplied by 100 was used to calculate the individual mortality percentage in each concentration.

2.9.1. Larval whole-body homogenate preparation and acetylcholinesterase assay

The departed larvae of *Anopheles stephensi* (3rd instar) exposed to AN-ZnO NPs for 24 h were retrieved, washed with distilled water to remove adherents, and blotted with tissue paper to withdraw moisture content. Then homogenized with ice-cold sodium phosphate buffer solution (20 mM, pH 7.4), centrifuged at 8000 rpm for 15 min and finally the supernatant was taken for enzyme assay.

2.9.2. Acetylcholinesterase (AChE) inhibition by AN-ZnO NPs

The protocol of Ellman *et al.,* (Ellman et al., 1961) with certain alterations was applied to assess the AChE inhibition activity of AN-ZnO NPs. Shortly, the solution of AChE (10 µL), AN-ZnO NPs (20 µL) of diverged concentrations and cold-phosphate buffer (150 µL) were placed in the 96-well microtiter plate followed by refrigeration (1–4 ℃). Then inhibitor of varying concentrations diluted in DMSO (0.1%), 0.4 mM acetylthiocholine iodide (20 µL) and DTNB (Ellman's reagent) was poured into each well. The reacting mixture was incubated at 37 ℃ for 30 min and the colour alteration (yellowish/ colourless) of the solution was recorded at 412 nm by a microplate reader. The inhibition % of the acetylcholinesterase enzyme by AN-ZnO NPs was calculated by applying the below-provided equation:

$$\text{Inhibition in } \% = \left[\left(C_{(Abs)} - S_{(Abs)}\right)\right]/C_{(A)}] \times 100$$

Here, $C_{(Abs)}$ = Control absorbance, $S_{(Abs)}$ = Sample absorbance.

2.9.3. Histological assessment of Anopheles stephensi

Histological analysis was executed to notify the alteration in the tissues of larvae. Both control larvae along with the AN-ZnO NPs exposed larvae (treated) of *Anopheles stephensi* mosquito were immersed in the fixative solution (10% formaldehyde), dehumidified with ethanol, cleansed with xylene solution, embedded in paraffin, and sectioned to get 5 µm thick tissue slices in a rotary ultramicrotome instrument. Paraffin was eradicated from the tissues and stained using Haematoxylin and Eosin stain and abnormalities were examined under an inverted microscope. The photographic images were captured with a digital camera.

2.10. Antibiofilm potentiality using microtiter plate assay

The antibiofilm efficacy of AN-ZnO NPs was executed by acquiring microtiter plate assay (MTP) as applied by Kumar *et al.,* (Kumar et al., 2012) with certain amendments. Shortly, 180 µL of Mueller-Hinton broth and 10 µL of overnight grown biofilm developing pathogenic bacterial cultures of *Staphylococcus aureus* (MTCC-3160) and *Klebsiella pneumoniae* (MTCC-432) were poured in a microtiter well individually and exposed with differing concentrations (1.17 µg/mL to 300 µg/mL) of AN-ZnO NPs along with the negative control (without nanoparticles) followed by maintenance at 37 ℃ for 24 h. Using 0.2 mL of PBS (phosphate buffer saline) removed unadhered bacteria. The adherent bacteria in the microtiter plate wall were further fixed by using 2% w/v of sodium acetate and stained using 0.1 % w/v of crystal violet. The extra stain was taken away by the complete washing with sterilized distilled water and left for drying. Then washed with 200 µL of ethanol (95% v/v) and finally, the absorbance was read at 595 nm using a microtiter plate reader. The inhibition % of the biofilm formation was computed by applying the formula:

$$\text{Biofilm inhibition}(\%) = [(Ac - As)]/Ac] \times 100$$

Here, A_C – Control absorbance, A_S- Sample absorbance.

2.11. Statistical analysis

Each experimental study was executed in three trials and the results were provided as mean ± standard deviation (SD). Graphpad Prism 9 software was applied for descriptive statistical analysis. Probit analysis was performed with NCSS 2021, v21.02 software for calculating LC_{50}, LC_{90} values. Data with probability (p) < 0.05 were taken to be statistically significant.

3. Result and discussions

3.1. Phytochemical screening

The scrutinizing of phytochemicals existing in the bark aqueous extract of *A.nilotica* was executed and the identified phytochemical's functional groups functioned as natural reducing and stabilizing factor in the fabrication of ZnO NPs (Table 1).

3.2. Visual observation and predictable mechanism in the genesis of AN-ZnO NPs

As a greener and eco-benefited avenue, ZnO NPs availing bark aqueous extract of *A.nilotica* was produced. The mild yellowish bark extract was turned into darkish brown on complete blending with zinc nitrate in 24 hrs (Fig. 1). This predicted the productive fabrication of ZnO NPs. Surface plasmon resonance (SPR) excitation attributed to the colour-shifting demonstrated AN-ZnO NPs genesis. The existed chemical group's electrons of plant bark extract were accountable for the biological reduction of zinc ion (Zn^{2+}) in

Table 1
Phytochemical scrutinized in the bark aqueous extract of *A.nilotica*.

Phytochemicals	Test executed	Inference achieved	Outcome
Alkaloids	Wagner test	Reddish-brown precipitate	Mildly occurred
Flavonoids	Lead acetate test	Yellow colour formation	Mildly occurred
Tannins	Ferric chloride test	Dark bluish colour	Copiously occurred
Carbohydrates	Molisch	A red cum violet ring development at the junction of two liquids	Slightly occurred
Phenols	Ellagic acid test	Muddy brownish colour	Mildly occurred

the zinc salt to nano zinc oxide. Therefore, concluded the function of bark extract as bio-reducer and stabilizing medium for nanoscale zinc oxide formation. Similarly, phyto-extract based colour shifting was detected in the study by Aminuzzaman *et al.,* (Aminuzzaman et al., 2018) in the ZnO NPs fabrication.

3.3. UV–Visible (UV–vis) spectroscopy of AN-ZnO NPs

UV–vis spectral analytical study is the most extensively applied optical technique to substantiate ZnO NPs formation by bioreduction. The synthesized AN-ZnO NPs were taken for UV–vis spectral analysis. The optical spectra of formed AN-ZnO NPs were noted periodically. An intensified peak at 350 nm substantiated the nanocrystal zinc oxide formation (Fig. 2). The bandgap computed through the *Tauc formula* was 3.55 eV (intrinsic bandgap). The outcome was in accordance with the previously availed data. In conformity to Gupta *et al.,* (Gupta et al., 2015); a systematic shift of absorption spectra wavelength to higher or lower happens with the diminution of nanoparticle size. Surface plasmon resonance impacts the shape and the nano dimension of the zinc oxide particles. Thus, a bold absorption spectra shift (blue shift) is confined to smaller size nanoparticles than an exciton Bohr radius of ZnO. UV–visible spectrum reported in our findings also correlated as experimented by already mentioned findings where phyto-inspired genesis of ZnO nanoparticles has been accomplished utilizing *Kalopanax septemlobus* and *Carica papaya* bark extract. The acquired AN-ZnO NPs were further characterized.

3.4. Fourier transform infrared (FTIR) spectral analysis of AN-ZnO NPs

The responsible chief chemical groups (minor/major) engaged to reduce zinc ions and capped zinc oxide nanoparticles in the bark

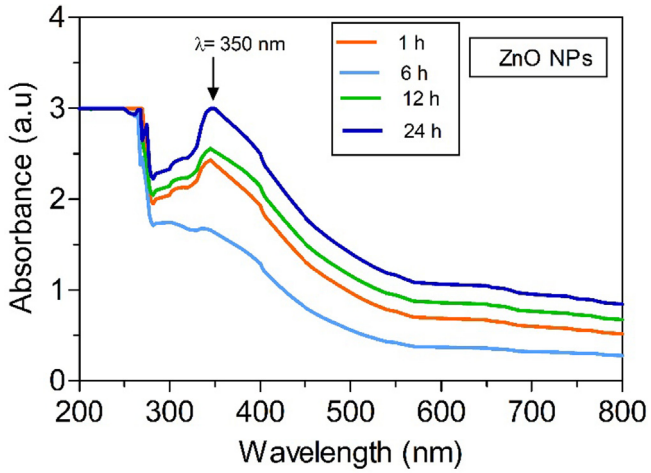

Fig. 2. UV–vis absorption spectrum of phytofabricated AN-ZnO NPs implementing *A.nilotica* bark extract.

of *A.nilotica* were unfolded in the FTIR spectroscopic analysis (Fig. 3). AN-ZnO NPs obtained a broad strong band at 3467 cm^{-1} indicated for O–H stretching owned to phenolic and alcoholic compounds. Two weak bands at 2923 cm^{-1} and 2850 cm^{-1} were implied for alkane and carboxylic groups (C–H vibrational asymmetric/symmetric stretching). Alkene group (C = C) was verified at 1623 cm^{-1}. The C-N vibration stretching of the aromatic ring in aromatic amine was represented at 1325 cm^{-1}. A band represented at 1130 cm^{-1} (C-O) for carboxylic and an ester group. Then at 620–440 cm^{-1} band (metal oxide stretching) was assigned to Zn-O stretching mode. A band achieved at 440 cm^{-1} further evinced the generation of AN-ZnO NPs by the display of vibrational Zn-O stretching trait. This was in parallelism to the before documented data on experimental grounds. The FTIR data reinforced the miscellaneous biochemical entities (proteins, alkaloids, polyphenols, flavonoids, terpenoids and carboxylic acids) that have been implicated in the plant-mediated greener route for synthesizing AN-ZnO NPs.

3.5. Powdered X-ray diffraction (P-XRD) spectral assessment of AN-ZnO NPs

The acquired diffraction patterns added knowledge on the existing phase chemistry, pureness, and crystalline trait of the AN-ZnO NPs. The XRD peak pattern of AN-ZnO NPs conveyed peak (2 theta) at 31.97°, 34.65°, 36.45°,47.63°,56.66°,62.87° and 67.84° that cognate to the crystalline phase (*hkl*) of 100, 002, 101, 102,

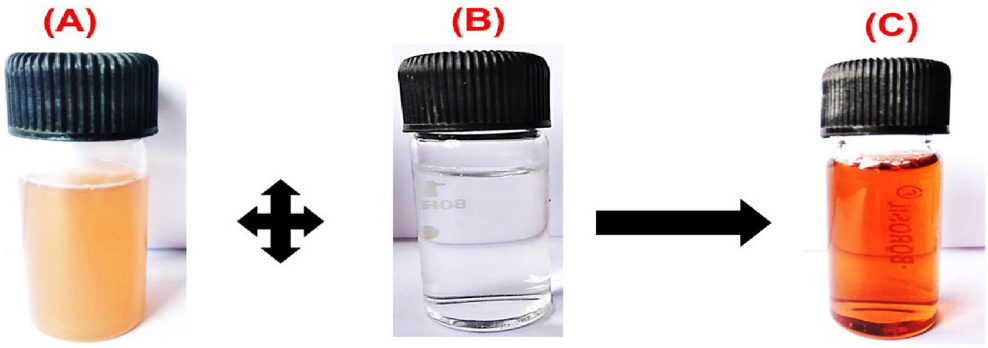

Fig. 1. Photograph revealing the visual colour change from mild yellowish to darkish-brown and fabrication of AN-ZnO NPs by blending (A) Bark (aqueous) extract of *A. nilotica* and (B) Zinc nitrate solution (C) Fabricated AN-ZnO NPs.

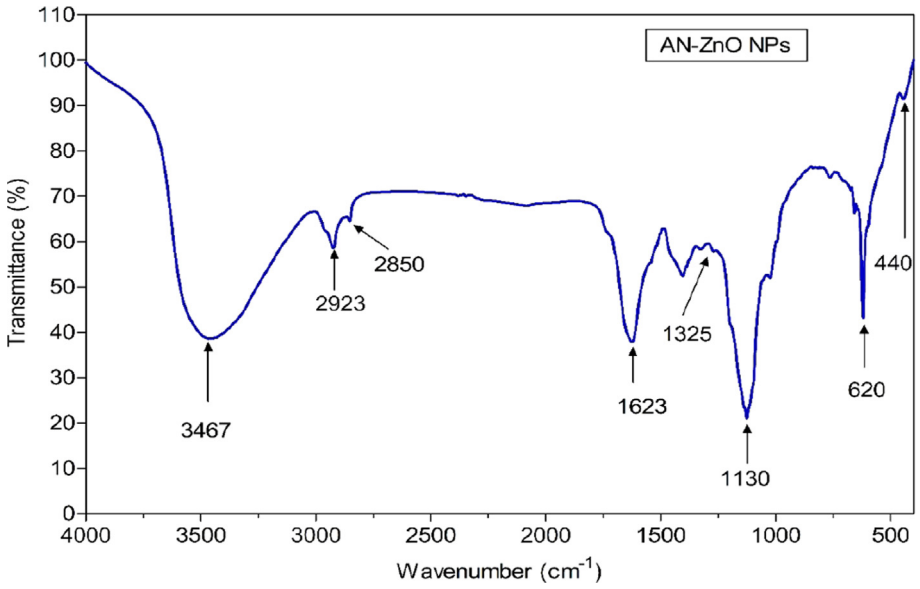

Fig. 3. Fourier transform infrared (FTIR) spectral analysis of AN-ZnO NPs.

110, 103 and 112 respectively and indexed to be the wurtzite or hexagonal feature of AN-ZnO NPs (Fig. 4). The crystallite dimension was computed, and the average grain size was calculated to be 39.01 nm (Table 2). The achieved sharp peaks matched with the standard JCPDS file number 89–0510. The AN-ZnO NPs size executed in the XRD was in correlation to the data obtained in TEM characterization.

3.6. SEM and EDX analysis of AN-ZnO NPs

Assessment of the surface structure of AN-ZnO NPs was done using scanning electron microscopy. Spherically and hexagonally shaped nano zinc oxide particles with non-uniformity, randomly arranged were pictured in the SEM micrographs was presented in Fig. 5(A). The particle size distribution was displayed in the Fig. 5(B). Aggregation of nanoparticles was spotted. The aggregation may be due to the occurrence of *Van-der-Waals* force between the nanoparticles. This sort of aggregation does not have any impression on particle stability. The obtained AN-ZnO NPs structures were in accordance as previously documented by Jayachandran *et al.,* (Jayachandran et al., 2021). The elemental composition yield of the AN-ZnO NPs was 63.07 % of zinc and

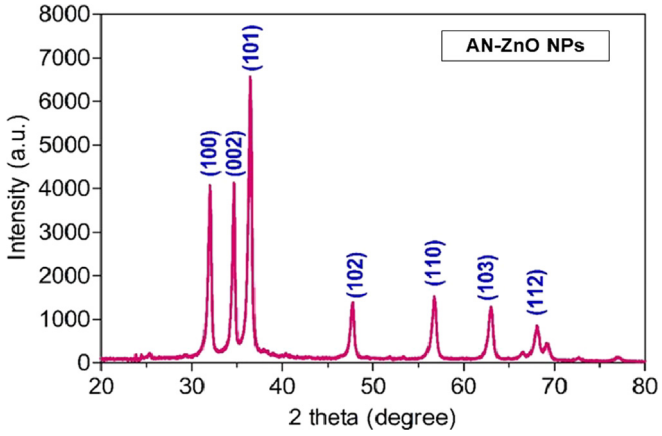

Fig. 4. Powdered-XRD spectral pattern of AN-ZnO NPs.

Table 2
Powdered XRD spectral analysis results at varying diffraction ranges (angles).

2θ	Lattice plane	FWHM in degree	Crystallite size in nm
31.97	100	0.231	37.35
34.65	002	0.193	45.02
36.45	101	0.243	35.94
47.63	102	0.268	33.83
56.66	110	0.292	32.27
62.87	103	0.210	46.30
67.84	112	0.236	42.36

36.93 % of oxygen in EDX Fig. 5(C). The lack of other elemental peaks justified the purity of AN-ZnO NPs. Already similar EDX elemental composition has been published in the work of Agarwal *et al.,* (Agarwal et al., 2019) and Fakhari *et al.,* (Fakhari et al., 2019).

3.7. High-resolution transmission electron microscopy (HR-TEM) and selected area electron diffraction (SAED) of AN-ZnO NPs

The surface morphology and size of the AN-ZnO NPs were proffered by high-resolution transmission electron microscopy (TEM). The micrograph of TEM manifested varied morphology like hexagonal and spherical for the AN-ZnO NPs. The average width size was calculated to be 35 nm respectively in Fig. 6(A). Vijayakumar *et al.,* (Vijayakumar et al., 2019), produced ZnO NPs from *Acalypha fruticosa* L leaf extract also illustrated similar morphology in TEM. As the synthesis was achieved in an aqueous medium, the particles owned higher surface energy which probably led to ZnO NPs agglomeration and even densification might also have trigger agglomeration causing confined space among the nanoparticles. This was displayed in the TEM micrograph. The calculated nanoparticle size in TEM complements the XRD results. Particularly, the hexagonal shape (Wurtzite shape) congruent to the pattern in XRD. High-resolution transmission electron microscopy (HR-TEM) micrograph with selected area diffraction pattern was depicted having the concentric ring with bright coloured spots that authenticated the nanocrystalline form of AN-ZnO NPs in Fig. 6(B). Previously, biogenically prepared ZnO NPs displayed a similar SAED pattern.

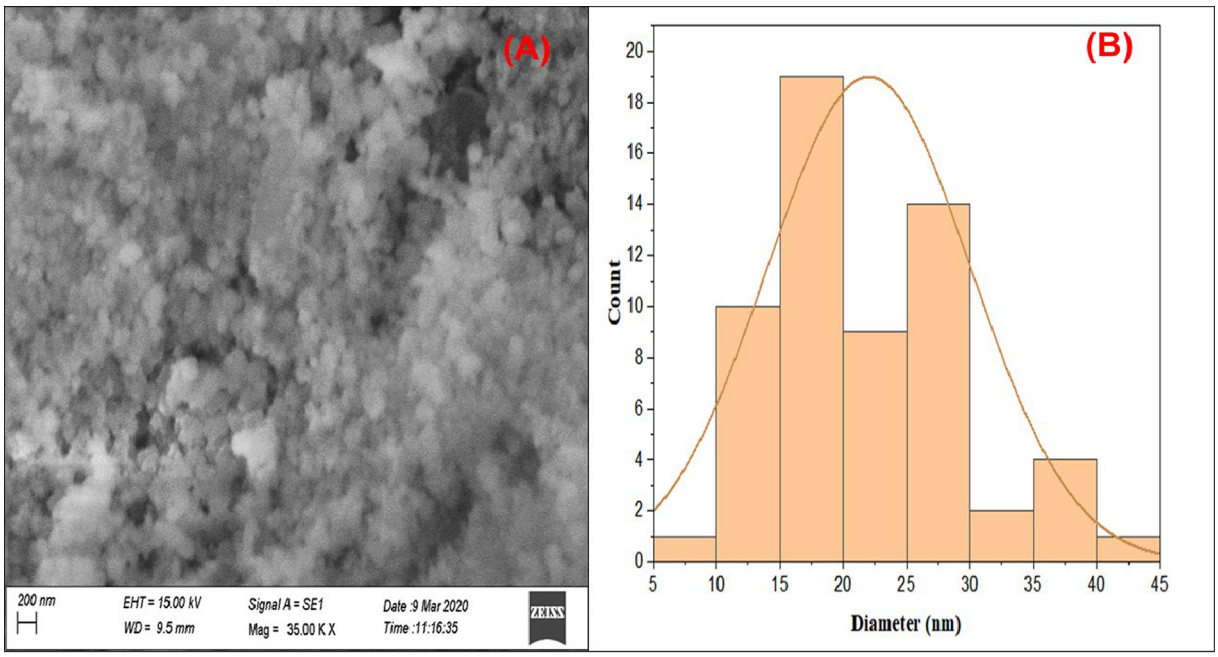

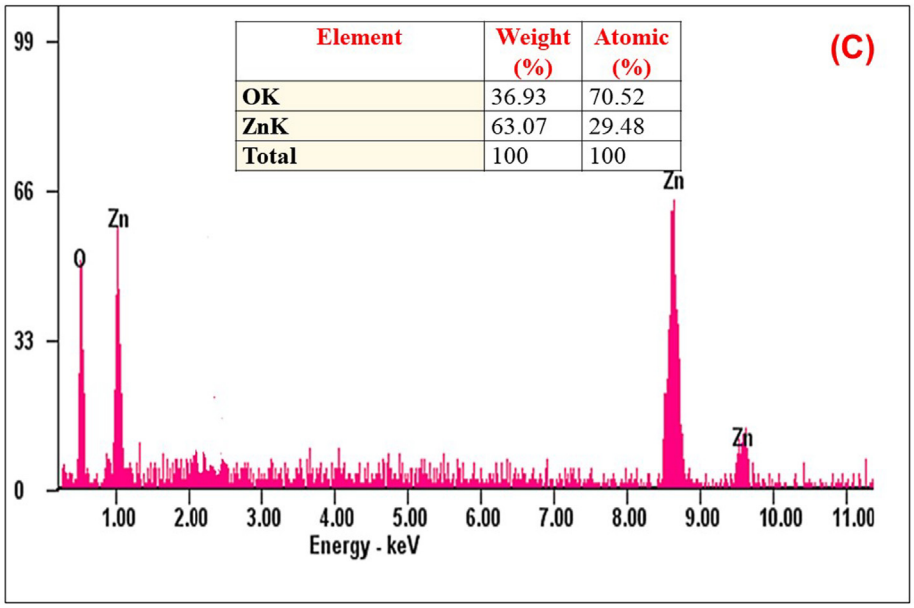

Fig. 5. (A) Scanning electron microscopic photographs of AN-ZnO NPs; (B) Histogram of SEM (C) EDX graph with elemental composition of phytofabricated An-ZnO NPs.

3.8. Antifungal susceptibility of AN-ZnO NPs

AN-ZnO NPs were analysed on the chosen pathogenic strains of fungi for fungicidal role using a well-diffusion method in the PDA media. The inhibition zone was achieved for each fungal strain at the desired varied concentrations of AN-ZnO NPs. There was a dose-mannered rise in the width of the inhibition zone for each tested fungal pathogen. The greatest inhibitory zone was achieved for *Candia albicans* (22.7 ± 0.32 mm) at 40 μg/mL followed by *Aspergillus flavus* (21.2 ± 0.22 mm), *Rhizopus oryzae* (18.3 ± 0.51 m m), *Aspergillus niger* (18.1 ± 0.76 mm) and *Trichophyton rubrum* (17. 6 ± 0.30 mm). Least width of inhibition zone was formed for *Microsporum gypseum* (15.3 ± 0.50 mm) at 40 μg/mL, respectively. The outcome of the tested AN-ZnO NPs at pathogenic fungal strains was revealed in Fig. 7 and Table 3, respectively. Amphotericin B was used as a comparative standard drug in this assay. Dobrucka *et al.*, (Dobrucka et al., 2018); also displayed a similar type of antifungal trait of *Chelidonium majus* extract bioformed ZnO NPs on the tested yeast, filamentous and dermatophytes as achieved in our test. Contact of zinc oxide nanoparticles with the fungal cell membrane causes an intracellular upsurge of reactive oxygen species (ROS), peroxidation of lipid content, distortion of protein and nucleic acid molecules, leading to entirely collapse of fungal membrane integrity and killing fungal cells via an apoptotic mechanism thus leakage of mitochondrial cytochrome. Also, it has been elucidated that phyto-involved ZnO NPs were able to arbitrate the swelling of fungal hyphae or expansion of its vacuoles, thus deforming the fungal architecture and ultimately causing fungal lysis.

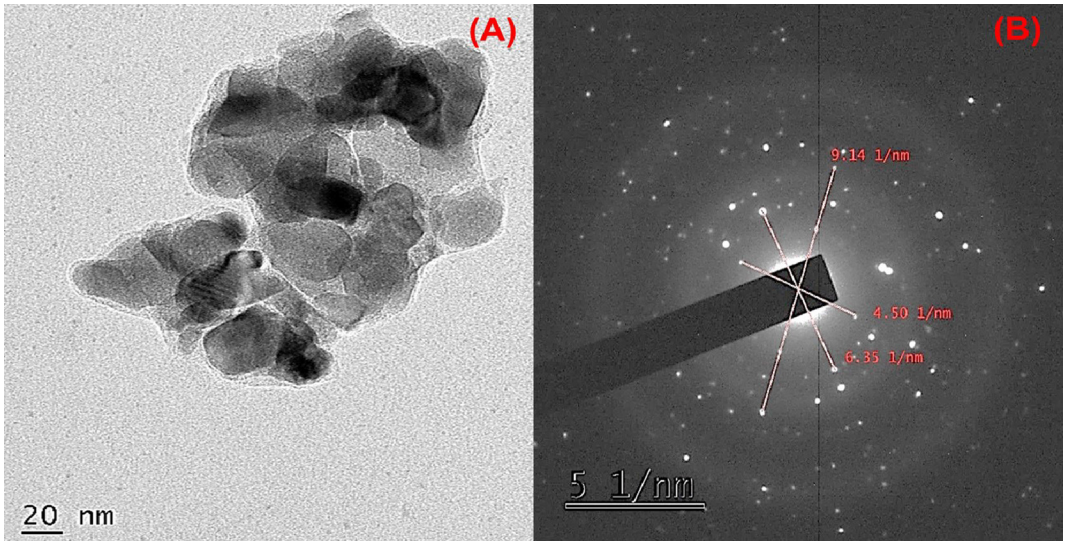

Fig. 6. (A) Transmission electron microscopy photograph of phytofabricated AN-ZnO NPs; (B) Selected area electron diffraction (SAED) pattern of AN-ZnO NPs.

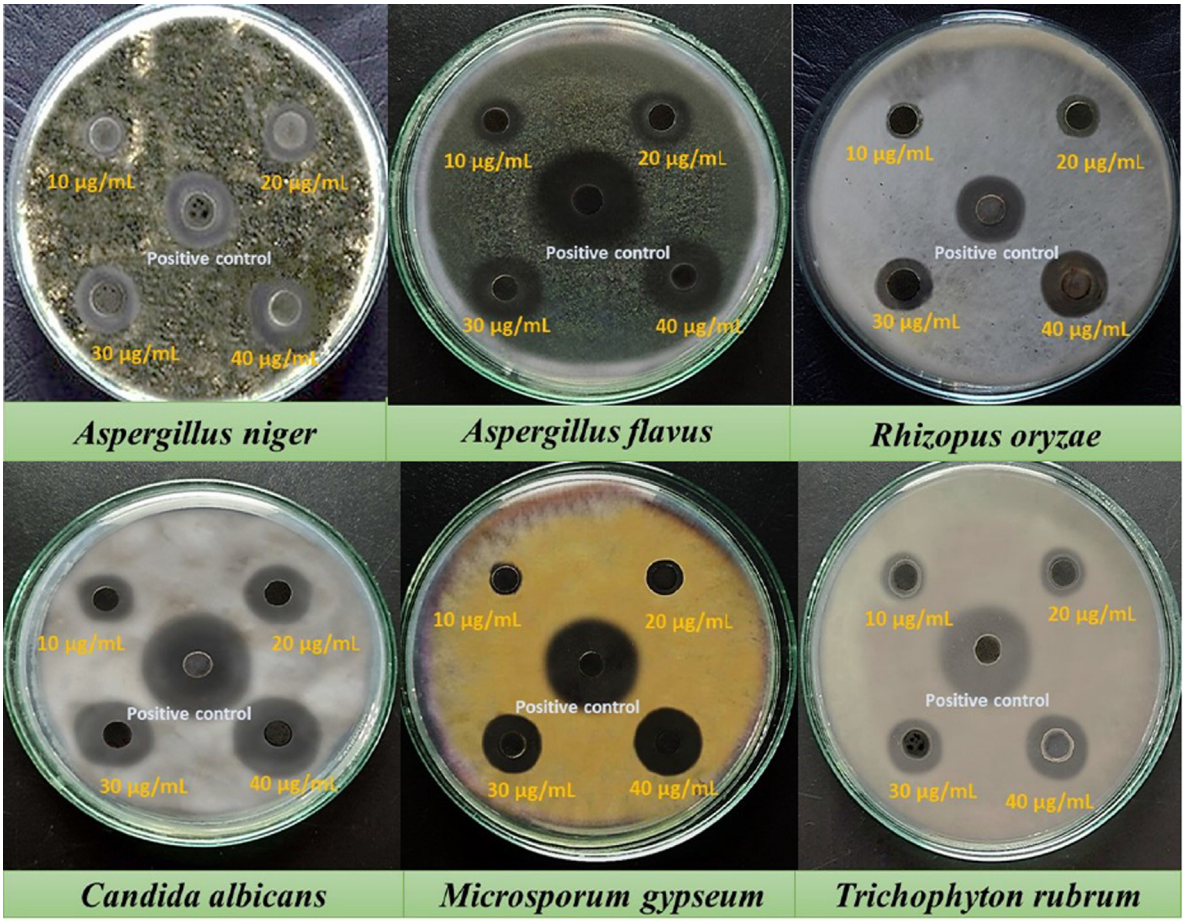

Fig. 7. Antifungal assay images of *A.nilotica* phytofabricated AN-ZnO NPs against the randomly chosen pathogenic fungal strains by agar well diffusion protocol.

The numerical reports (n = 3 trials) are given as mean ± standard deviation (Mean ± SD).

The supplementary section of the manuscript discusses further analysis to understand the complete biological activities that include (i) antioxidant assessment and (ii) cytotoxic assessment.

4. Conclusion

Phyto nanotechnology has superiority over the intricate physicochemical methodologies for nanoparticle fabrication. Herein, zinc oxide nanoparticles were harnessed extracellularly implementing the medicinally worthy *A.nilotica* bark aqueous extract in a

Table 3
Fungicidal activity of AN-ZnO NPs on diverged range of pathogenic strains of fungi.

Fungal strains	Inhibition zone size in mm				
	10 μg/mL	20 μg/mL	30 μg/mL	40 μg/mL	Amphotericin B(10 μg/mL)
Aspergillus niger	12.0 ± 0.00	14.2 ± 0.80	17.0 ± 0.27	18.1 ± 0.76	20.3 ± 0.52
Aspergillus flavus	13.1 ± 0.72	16.3 ± 0.57	19.4 ± 0.59	21.2 ± 0.22	28.3 ± 0.73
Rhizopus oryzae	10.2 ± 0.51	12.0 ± 0.44	16.3 ± 0.29	18.3 ± 0.51	19.0 ± 0.86
Candida albicans	14.3 ± 0.60	17.5 ± 0.30	19.1 ± 0.87	22.7 ± 0.32	27.0 ± 0.90
Microsporum gypseum	9.0 ± 0.32	11.5 ± 0.73	13.1 ± 0.00	15.3 ± 0.50	22.1 ± 0.56
Trichophyton rubrum	10.4 ± 0.51	12.2 ± 0.48	14.4 ± 0.63	17.6 ± 0.30	24.3 ± 0.49

lower-budget, eco-sustainable way without the applications of noxious chemicals. As disclosed in the FTIR report, the plant bioactive natural chemical groups provided multiple traits as bioreducer, stabilizer, and capping factor in nanoparticle fabrication. The advanced characterization tools pinpointed the crystalline trait, spherical and hexagonal morphological features of AN-ZnO NPs with an average size of 35 nm. The fabricated AN-ZnO NPs presented astounding antifungal activity towards the tested fungal pathogenic strains. The antioxidant property of AN-ZnO NPs were clearly concentration-based. On MCF-7 cell line, AN-ZnO NPs presented cytotoxic trait tested by MTT assay. ROS origination, membrane distortion in mitochondria and nuclear fragmentation were the chief factors for the cytotoxic trait of AN-ZnO NPs in a dose-mannered. Inhibitory role on acetylcholinesterase (AChE) enzyme was achieved on AN-ZnO NPs exposure to the *Anopheles stephensi* larvae on dose-credential. Additionally, biofilm development was hindered when AN-ZnO NPs reacted with pathogenic biofilm generating bacterial species such as *Staphylococcus aureus* and *Klebsiella pneumoniae*. Comprehensively, the bioactivities displayed in our report, conclude that AN-ZnO NPs may be practiced in the bio nanomedicine province as an amendatory for health illness. Also, pave a new route for eradicating mosquitoes with nano-larvicidal trait. To relate and understand the in-depth of bioactivities of AN-ZnO NPs, in vivo experimentation must be executed in future.

Declaration of Competing Interest

The authors declare that they have no known competing financial interests or personal relationships that could have appeared to influence the work reported in this paper.

Acknowledgement

All the authors are thankful to the Department of Biotechnology, Thiruvalluvar University, Serkkadu, Vellore, Tamil Nadu, India for furnishing laboratory facilities for executing the research experimental studies.

Appendix A. Supplementary material

Supplementary data to this article can be found online at https://doi.org/10.1016/j.jksus.2023.102753.

References

Agarwal, H., Nakara, A., Menon, S., Shanmugam, V.K., 2019. Eco-friendly synthesis of zinc oxide nanoparticles using Cinnamomum Tamala leaf extract and its promising effect towards the antibacterial activity. J. Drug Deliv. Sci. Technol. 53, 35.

Aminuzzaman, M., Ying, L.P., Goh, W.S., Watanabe, A., 2018. Green synthesis of zinc oxide nanoparticles using aqueous extract of Garcinia mangostana fruit pericarp and their photocatalytic activity. Bull. Mater. Sci. 41, 76.

Angel Ezhilarasi, A., Judith Vijaya, J., Kaviyarasu, K., John Kennedy, L., Ramalingam, R.J., Al-Lohedan, H.A., 2018. Green synthesis of NiO nanoparticles using Aegle marmelos leaf extract for the evaluation of in-vitro cytotoxicity, antibacterial and photocatalytic properties. J. Photochem. Photobiol. B Biol. 180, 39–50.

Dobrucka, R., Dlugaszewska, J., Kaczmarek, M., 2018. Cytotoxic and antimicrobial effects of biosynthesized ZnO nanoparticles using of Chelidonium majus extract. Biomed. Microdevices. 20, 67.

Ellman, G.L., Courtney, K.D., Andres Jr, V., Featherstone, R.M., 1961. Biochem. Pharmacol. 88, 88–99.

Ezhilarasi, A.A., Vijaya, J.J., Kennedy, L.J., Kaviyarasu, K., 2019. Green mediated NiO nano-rods using Phoenix dactylifera (Dates) extract for biomedical and environmental applications. Mater. Chem. Phys. 241, 122419.

Fakhari, S., Jamzad, M., Kabiri Fard, H., 2019. Green synthesis of zinc oxide nanoparticles: a comparison. Green Chem. Lett. Rev. 12, 19–24.

Gao, Y., Han, Y., Cui, M., Tey, H.L., Wang, L., Xu, C., 2017. ZnO nanoparticles as an antimicrobial tissue adhesive for skin wound closure. J. Mater. Chem. B. 5, 4535–4541.

Garg, A., Sharma, G.S., Goyal, A.K., Ghosh, G., Si, S.C., Rath, G., 2020. Recent advances in topical carriers of anti-fungal agents. Heliyon. 6, e04663.

Gupta, A., Srivastava, P., Bahadur, L., Amalnerkar, D.P., Chauhan, R., 2015. Comparison of physical and electrochemical properties of ZnO prepared via different surfactant-assisted precipitation routes. Appl. Nanosci. 5, 787–794.

Jayachandran, A., Aswathy, T.R., Nair, A.S., 2021. Green synthesis and characterization of zinc oxide nanoparticles using Cayratia pedata leaf extract. Biochem. Biophys. Reports. 26, 100995.

Jegadeesan, G.B., Srimathi, K., Santosh Srinivas, N., Manishkanna, S., Vignesh, D., 2019. Green synthesis of iron oxide nanoparticles using Terminalia bellirica and Moringa oleifera fruit and leaf extracts: antioxidant, antibacterial and thermoacoustic properties. Biocatal. Agric. Biotechnol. 21, 57–69.

Khader, A., Arinzeh, T.L., 2020. Biodegradable zinc oxide composite scaffolds promote osteochondral differentiation of mesenchymal stem cells. Biotechnol. Bioeng. 117, 194–209.

Khandel, P., Yadaw, R.K., Soni, D.K., Kanwar, L., Shahi, S.K., 2018. Biogenesis of Metal Nanoparticles and Their Pharmacological Applications: Present Status and Application Prospects. Springer, Berlin Heidelberg.

Kumar, P., Senthamilselvi, S., Lakshmipraba, A., Premkumar, K., Muthukumaran, R., Visvanathan, P., Ganeshkumar, R.S., Govindaraju, M., 2012. Efficacy of bio-synthesized silver nanoparticles using Acanthophora spicifera to encumber biofilm formation. Dig. J. Nanomater. Biostructures. 7, 511–522.

Kuppurangan, G., Karuppasamy, B., Nagarajan, K., Krishnasamy Sekar, R., Viswaprakash, N., Ramasamy, T., 2016. Biogenic synthesis and spectroscopic characterization of silver nanoparticles using leaf extract of Indoneesiella echioides: in vitro assessment on antioxidant, antimicrobial and cytotoxicity potential. Appl. Nanosci. 6, 973–982.

Kuppusamy, P., Yusoff, M.M., Maniam, G.P., Govindan, N., 2016. Biosynthesis of metallic nanoparticles using plant derivatives and their new avenues in pharmacological applications - An updated report. Saudi Pharm. J. 24, 473–484.

Mani, M., Okla, M.K., Selvaraj, S., Kumar, A.R., Kumaresan, S., Muthukumaran, A., Kaviyarasu, K., El-Tayeb, M.A., Elbadawi, Y.B., Almaary, K.S., Almunqedhi, B.M.A., 2021. A novel biogenic Allium cepa leaf mediated silver nanoparticles for antimicrobial, antioxidant, and anticancer effects on MCF-7 cell line. Environ. Res. 198, 111199.

Mani, M., Pavithra, S., Mohanraj, K., Kumaresan, S., Alotaibi, S.S., Eraqi, M.M., Dhanesh Gandhi, A., Babujanarthanam, R., Maaza, M., Kaviyarasu, K., 2021. Studies on the spectrometric analysis of metallic silver nanoparticles (Ag NPs) using Basella alba leaf for the antibacterial activities. Environ. Res. 199, 111274.

Mani, M., Harikrishnan, R., Purushothaman, P., Pavithra, S., Rajkumar, P., Kumaresan, S., Al, D.A., Farraj, M.S., Elshikh, B., Balasubramanian, K.K., 2021. Systematic green synthesis of silver oxide nanoparticles for antimicrobial activity. Environ. Res. 202, 111627.

Mayedwa, N., Mongwaketsi, N., Khamlich, S., Kaviyarasu, K., Matinise, N., Maaza, M., 2018. Green synthesis of nickel oxide, palladium and palladium oxide synthesized via Aspalathus linearis natural extracts: physical properties & mechanism of formation. Appl. Surf. Sci. 446, 266–272.

Menon, S., Shanmugam, V.K., 2020. Cytotoxicity analysis of biosynthesized selenium nanoparticles towards A549 lung cancer cell line. J. Inorg. Organomet. Polym. Mater. 30, 1852–1864.

Patil, S., Chandrasekaran, R., 2020. Biogenic nanoparticles: a comprehensive perspective in synthesis, characterization, application and its challenges. J. 18, 179.

Punniyakotti, P., Panneerselvam, P., Perumal, D., Aruliah, R., Angaiah, S., 2020. Anti-bacterial and anti-biofilm properties of green synthesized copper nanoparticles

from Cardiospermum halicacabum leaf extract. Bioprocess Biosyst. Eng. 43, 1649–1657.
Rajeswari, M., Agrawal, P., Roopa, G.S., Akshay Jain, A., Kumar Gupta, P., 2018. Green synthesis and characterization of multifunctional zinc oxide nanomaterials using extract of Moringa Oleifera Seed. Mater. Today Proc. 5, 20996–21002.
Rawani, A., 2017. Mosquito larvicidal activity of green silver nanoparticle synthesized from extract of bud of Polianthus tuberosa L. Int. J. Nanotechnol. Appl. 15, 17–28.
Sathiyaraj, S., Suriyakala, G., Dhanesh Gandhi, A., Babujanarthanam, R., Kaviyarasu, K., Rajakrishnan, R., Kuppusamy, P., B. Ebanda Kedi Philippe,, 2022. Chemical composition and mosquitocidal efficacy of panchagavya against Anopheles stephensi, Aedes aegypti and Culex quinquefasciatus. J. King Saud Univ. – Sci. 34, 101960.
Senguttuvan, J., Paulsamy, S., Karthika, K., 2014. Phytochemical analysis and evaluation of leaf and root parts of the medicinal herb, Hypochaeris radicata L. for in vitro antioxidant activities, Asian Pac. J Trop. Biomed. 4, S359–S367.
Subramanian, R., Subbramaniyan, P., Raj, V., 2013. Antioxidant activity of the stem bark of Shorea roxburghii and its silver reducing power. Springer. 2, 1–11.
Sundraraman, G., Jayakumari, L.S., 2020. Meticulous Taxifolin releasing performance by the zinc oxide nanoparticles: as a short road to drug delivery system for cancer therapeutics. J. Clust. Sci. 31, 241–255.
Sylvie, D.D., Anatole, P.C., Cabral, B.P., Veronique, P.B., 2014. Comparison of in vitro antioxidant properties of extracts from three plants used for medical purpose in Cameroon: Acalypha racemosa, Garcinia lucida and Hymenocardia lyrata, Asian Pac. J Trop. Biomed. 4, S625–S632.
Valsalam, S., Agastian, P., Arasu, M.V., Al-Dhabi, N.A., Ghilan, A.K.M., Kaviyarasu, K., 2019. Rapid biosynthesis and characterization of silver nanoparticles from the leaf extract of Tropaeolum majus L. and its enhanced in-vitro antibacterial, antifungal, antioxidant and anticancer properties. J. Photochem. J. Photochem. Photobiol. B: Biol. 191, 65–74.
Vijayakumar, S., Arulmozhi, P., Kumar, N., Sakthivel, B., Prathip Kumar, S., Praseetha, P.K., Acalypha fruticosa L., 2019. Leaf extract mediated synthesis of ZnO nanoparticles: characterization and antimicrobial activities. Mater. Today Proc. 23, 73–80.
World Health Organization (WHO), Communicable Disease Tool Kit, World Health Organization, Sudan, 2005. WHO/CDS/2005.26.